STRUCTURAL SCIENCE
CRYSTAL ENGINEERING
MATERIALS

ISSN 2052-5206

Deformations of the α-Fe_2O_3 rhombohedral lattice across the Néel temperature

P. Fabrykiewicz,[a] M. Stękiel,[a,b] I. Sosnowska[a] and R. Przeniosło[a]*

[a]Faculty of Physics, University of Warsaw, Pasteura 5, 02-093 Warsaw, Poland, and [b]Institute of Geosciences, Goethe University, D-60438 Frankfurt am Main, Germany. *Correspondence e-mail: radek@fuw.edu.pl

Received 15 July 2016
Accepted 8 November 2016

Edited by M. de Boissieu, SIMaP, France

Keywords: Néel temperature; high-resolution synchrotron powder diffraction; peak-broadening; ferromagnetism.

CCDC references: 1515808; 1515809

Supporting information: this article has supporting information at journals.iucr.org/b

High-resolution synchrotron radiation powder diffraction patterns of α-Fe_2O_3 measured between room temperature and 1100 K, *i.e.* above the Néel temperature T_N = 950 K, have been analyzed. The integral breadths of the Bragg peaks show a *hkl*-dependent anisotropy, both below and above T_N. This anisotropy can be quantitatively described by using a statistical peak-broadening model [Stephens (1999). *J. Appl. Cryst.* **32**, 281]. Model calculations show that the rhombohedral α-Fe_2O_3 lattice is deformed and the deformation leads to a monoclinic lattice with the unique monoclinic axis along the hexagonal [110] direction both below and above T_N. The monoclinic symmetry of bulk α-Fe_2O_3 is compatible with α-Fe_2O_3 nanowire growth along the [110] direction reported in Fu *et al.* [*Chem. Phys. Lett.* (2001), **350**, 491].

1. Introduction

Antiferromagnetic and canted weak ferromagnetic states (Néel & Pauthenet, 1952; Dzyaloshinsky, 1958; Moriya, 1960) as well as spin-reorientation phenomena (Morin, 1950) were discovered in early studies of hematite, α-Fe_2O_3 (Morrish, 1994). The crystal structure of α-Fe_2O_3 is of corundum-type with trigonal symmetry (Shull *et al.*, 1951; Maslen *et al.*, 1994; Petrás *et al.*, 1996; Hill *et al.*, 2008). Recent structural studies have shown that the crystal structure of α-Fe_2O_3 is monoclinic at room temperature (Przeniosło *et al.*, 2014). The monoclinic symmetry of the α-Fe_2O_3 crystal structure is compatible with the canted antiferromagnetic ordering (Przeniosło *et al.*, 2014; Stękiel *et al.*, 2015), while the trigonal corundum-type crystal structure is not. There are also other arguments supporting the hypothesis of a monoclinic symmetry of the α-Fe_2O_3 crystal structure. The α-Fe_2O_3 nanowires and nanobelts (Fu *et al.*, 2001; Wen *et al.*, 2005; Yuan *et al.*, 2012) are elongated objects which grow along the [110] (hexagonal) direction, *i.e.* along the unique monoclinic $\mathbf{b}_m$ axis. The choice of the [110] growth direction indirectly points to a possible breaking of the threefold rotation symmetry of the α-Fe_2O_3 crystal structure.

It is often assumed, see *e.g.* Grimmer (2015), that the small monoclinic distortions of the crystal structure of α-Fe_2O_3 observed at room temperature are due to the magnetic ordering. This idea is in agreement with the Landau description of phase transitions (Landau & Lifschitz, 1969) assuming that the symmetry of the paramagnetic phase (at high temperature) and the symmetry of the magnetically ordered phase (at low temperature) should show a group–subgroup relation. The paper is motivated by the following question. Does the crystal structure symmetry of α-Fe_2O_3 change around the magnetic phase transition at T_N = 950 K?

Recent structural studies of other magnetic materials, *e.g.* $BiFeO_3$ (Sosnowska *et al.*, 2012) and Cr_2O_3 (Stękiel *et al.*,

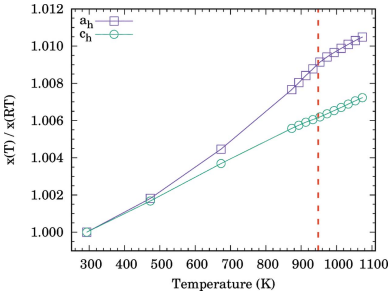

2015), have also shown monoclinic deformations of the rhombohedral lattice. In the case of $BiFeO_3$ the magnetic moments modulation directed along the hexagonal [110] direction (Sosnowska *et al.*, 1982) favor the monoclinic space group *Cc* over the trigonal *R*3*c* (Sosnowska *et al.*, 2012). The observation of small antiferromagnetic contributions perpendicular to the hexagonal [001] direction in Cr_2O_3 (Brown *et al.*, 1999, 2002) also favor the monoclinic symmetry over the trigonal one.

2. Experimental

High-resolution synchrotron radiation diffraction measurements were performed with a synthetic commercial α-Fe_2O_3 powder sample provided by Aldrich. The measurements were performed at the ESRF beamline ID22 operating at the wavelength 0.40086 Å, as described in Stępkiel *et al.* (2015). Synchrotron radiation diffraction measurements were performed with α-Fe_2O_3 at several temperature steps by warming from room temperature to 1053 K. After reaching every temperature step by the hot-air blower sensor there was a 12 min waiting time before thermal equilibration. Synchrotron radiation powder diffraction measurements with α-Fe_2O_3 took 30 min at every temperature step. The angular range was $5 < 2\theta < 30^\circ$ corresponding to $0.218 < s < 1.291$ Å^{-1}, where $s = 2\sin(\theta)/\lambda$, covering 80 Bragg reflections of the trigonal crystal structure of α-Fe_2O_3. Polycrystalline powder samples were sealed in 0.5 mm diameter borosilicate capillaries. The capillaries were rotated in order to reduce potential texture effects. The synchrotron radiation powder diffraction patterns of α-Fe_2O_3 were analyzed by the Rietveld method asuming the corundum-type crystal structure (space group $R\bar{3}c$) and the distorted monoclinc crystal structure (space group $C2/c$) as described in Przeniosło *et al.* (2014). The hexagonal setting of the space group $R\bar{3}c$ will be used in the present paper.

3. Results

3.1. Monoclinic crystal structure model

The synchrotron radiation diffraction patterns of α-Fe_2O_3 were analyzed by the Rietveld method using *JANA*2006 (Petříček *et al.*, 2014), assuming both rhombohedral (space group $R\bar{3}c$) and monoclinic (space group $C2/c$) lattices. The relation between the monoclinic lattice vectors: $\mathbf{a}_m^0$, $\mathbf{b}_m^0$ and $\mathbf{c}_m^0$ and the rhombohedral lattice vectors (in a hexagonal setting) $\mathbf{a}_h^0$, $\mathbf{b}_h^0$ and $\mathbf{c}_h^0$ is (Sosnowska *et al.*, 2012)

$$\mathbf{a}_m^0 = -\frac{1}{3}\mathbf{a}_h^0 + \frac{1}{3}\mathbf{b}_h^0 - \frac{2}{3}\mathbf{c}_h^0, \quad (1)$$

$$\mathbf{b}_m^0 = -\mathbf{a}_h^0 - \mathbf{b}_h^0, \quad (2)$$

$$\mathbf{c}_m^0 = \mathbf{c}_h^0. \quad (3)$$

The splitting of Wyckoff positions between $R\bar{3}c$ and $C2/c$ space groups for α-Fe_2O_3 is shown in Table 1. There is only one positional parameter for oxygen ions x(O) in the trigonal structure model of α-Fe_2O_3. The present paper describes a study of the Bragg peak shapes which give information about the lattice deformations.

Table 1
Splitting of the Wyckoff positions between the $R\bar{3}c$ (hexagonal setting) and the $C2/c$ (monoclinic) space groups for α-Fe_2O_3.

$C2/c$ (equiv.) shows the monoclinic coordinates which are obtained from the rhombohedral ones by using transformation (1)–(3). The last column shows which coordinates are free in $C2/c$.

Ion	$R\bar{3}c$		$C2/c$ (equiv.)		$C2/c$ (general)
Fe	12*c*	$(0, 0, z_0)$	8*f*	$(0, 0, z_0)$	$(0, 0, z)$
O	18*e*	$(x_0, 0, \frac{1}{4})$	8*f*	$(-\frac{3}{2}x_0, -\frac{1}{2}x_0, \frac{1}{4} - x_0)$	(x, y, z)
O	18*e*	$(\bar{x}_0, \bar{x}_0, \frac{1}{4})$	4*e*	$(0, x_0, \frac{1}{4})$	$(0, y, \frac{1}{4})$

The index '0' in equations (1)–(3) means that both the hexagonal and monoclinic lattice vectors correspond to the rhombohedral lattice, while the index '1' refers to the monoclinic lattice (distorted with regard to the rhombohedral one), also called a pseudo-hexagonal lattice.

For the Rietveld refinement asssuming the monoclinic space group $C2/c$ the starting values of the lattice parameters are a_m^0, b_m^0, c_m^0 and β_m^0, and the final parameters are a_m^1, b_m^1, c_m^1 and β_m^1. The oxygen atomic coordinates obtained with the trigonal structure were transformed to the monoclinic lattice, as given in Table 1, and these were the starting values for the refinements of the monoclinic model. The oxygen coordinates of (4*e*) and (8*f*) positions (shown in Table 1) were free in the Rietveld fits with the monoclinic structure model. Isotropic atomic displacement parameters for Fe and O ions were refined both in the trigonal and monoclinic models. The isotropic peak width dependence from Caglioti *et al.* (1958) was assumed

$$FWHM^2(\theta) = U\tan^2(\theta) + V\tan(\theta) + W. \quad (4)$$

The temperature dependence of the relative elongation of the hexagonal unit-cell parameters of α-Fe_2O_3, *i.e.* $a_h(T)/a_h(RT)$

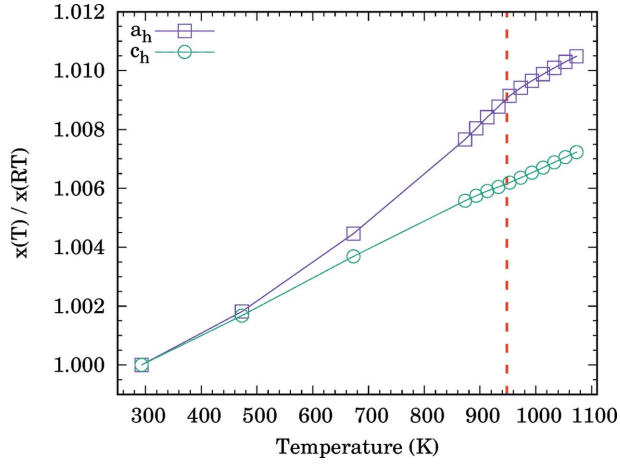

Figure 1
Temperature dependence of the relative elongation of the α-Fe_2O_3 hexagonal lattice parameters a_h^0 and c_h^0 obtained from Rietveld refinement of synchrotron radiation diffraction data. The vertical dotted line denotes the Néel temperature T_N = 950 K.

Table 2
Structural parameters for α-Fe_2O_3 obtained at 293 K for the monoclinic model and the trigonal model (see text).

The last column gives the relative change of each parameter.

Parameter	Monoclinic (index 1) pseudo-hexagonal	Trigonal (index 0) hexagonal	Relative change $(x^1_m - x^0_m)/x^0_m \times 10^6$
$\mathbf{a}_m$ (Å)	9.61865 (38)	9.61769 (11)	100 (14)
$\mathbf{b}_m$ (Å)	5.03554 (11)	5.03589 (4)	−70 (9)
$\mathbf{c}_m$ (Å)	13.75158 (55)	13.75154 (14)	3 (13)
β_m (°)	162.404 (1)	162.403 (2)	2 (13)
$\mathbf{a}_h$ (Å)	5.03610 (4)	5.03589 (4)	42 (8)
$\mathbf{b}_h$ (Å)	5.03610 (4)	5.03589 (4)	42 (8)
$\mathbf{c}_h$ (Å)	13.75158 (13)	13.75154 (14)	3 (13)
α_h (°)	90.0154 (20)	90.0	171 (23)
β_h (°)	89.9846 (20)	90.0	−171 (23)
γ_h (°)	120.0073 (6)	120.0	61 (5)

Table 3
Structural parameters for α-Fe_2O_3 obtained at 1053 K for the monoclinic model and the trigonal model (see text).

The last column gives the relative change of each parameter.

Parameter	Monoclinic (index 1) pseudo-hexagonal	Trigonal (index 0) hexagonal	Relative change $(x^1_m - x^0_m)/x^0_m \times 10^6$
$\mathbf{a}_m$ (Å)	9.68920 (55)	9.68845 (40)	77 (20)
$\mathbf{b}_m$ (Å)	5.08737 (15)	5.08774 (13)	−72 (13)
$\mathbf{c}_m$ (Å)	13.84868 (71)	13.84864 (57)	3 (17)
β_m (°)	162.351 (1)	162.350 (13)	−1 (19)
$\mathbf{a}_h$ (Å)	5.08796 (3)	5.08774 (13)	43 (14)
$\mathbf{b}_h$ (Å)	5.08796 (3)	5.08774 (13)	43 (14)
$\mathbf{c}_h$ (Å)	13.84868 (11)	13.84864 (57)	3 (17)
α_h (°)	90.0115 (18)	90.0	127 (20)
β_h (°)	89.9885 (18)	90.0	−127 (20)
γ_h (°)	120.0077 (4)	120.0	64 (4)

and $c_h(T)/c_h(RT)$ is shown in Fig. 1. These results are similar to those from Petrás *et al.* (1996), which also show a change of the slope of $a_h(T)$ and $c_h(T)$ near T_N = 950 K.

The monoclinic unit cell is difficult to visualize and in order to show its main properties a transformation to the pseudo-hexagonal axes was performed. This was done by taking a^1_m, b^1_m, c^1_m and β^1_m and using inverted equations (1)–(3) to obtain the pseudo-hexagonal lattice parameters: $a^1_h = b^1_h$, c^1_h, α^1_h, β^1_h and γ^1_h. Please note that in the pseudo-hexagonal lattice it is possible that $\alpha^1_h \neq 90°$ or $\beta^1_h \neq 90°$ or $\gamma^1_h \neq 120°$. The values of the lattice parameters for α-Fe_2O_3 at room temperature and 1053 K are given in Tables 2 and 3, respectively. The values of a_h and c_h at room temperature and 1053 K given in Petrás *et al.* (1996) agree reasonably with those given in Tables 2 and 3. The refined atomic coordinates are given in Table 4.

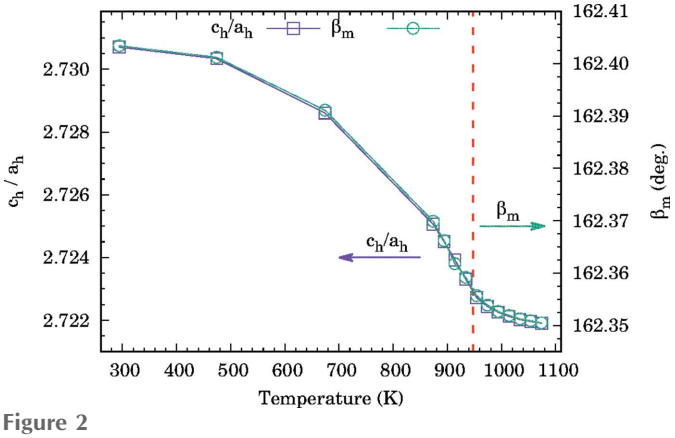

Figure 2
The temperature dependence of the ratio of the hexagonal lattice parameters c^0_h/a^0_h (left scale) is compared with the temperature dependence of the monoclinic angle β^1_m (right scale). The vertical dotted line denotes the Néel temperature T_N = 950 K.

Table 4
Atomic coordinates and isotropic displacement parameters obtained from Rietveld refinement for α-Fe_2O_3 by assuming the monoclinic structure model at 293 K and 1053 K.

	293 K	1053 K
z(Fe) (8f)	0.14473 (3)	0.14425 (3)
y(O) (4e)	0.309 (3)	0.313 (3)
x(O) (8f)	−0.449 (2)	−0.449 (3)
y(O) (8f)	−0.156 (2)	−0.155 (3)
z(O) (8f)	−0.050 (2)	−0.049 (2)
U_{iso} (Fe)	0.0033 (17)	0.0131 (28)
U_{iso} (O)	0.0005 (60)	0.0102 (90)

The temperature dependence of the hexagonal unit parameters' ratio c^0_h/a^0_h is similar to that of the monoclinic β^1_m angle as shown in Fig. 2. There is an inflection point of both c^0_h/a^0_h and β^1_m near T_N indicating the importance of spin-lattice coupling in α-Fe_2O_3 as shown earlier in Petrás *et al.* (1996). The relative size of the monoclinic deformation is estimated by calculating the relative change of the monoclinic unit-cell parameters with regard to the trigonal ones, *e.g.* $(a^1_m - a^0_m)/a^0_m \times 10^6$. There is a positive change of a_m and a negative change of b_m (both larger than the statistical errors), while the values of c_m and β_m do not change within errors. The

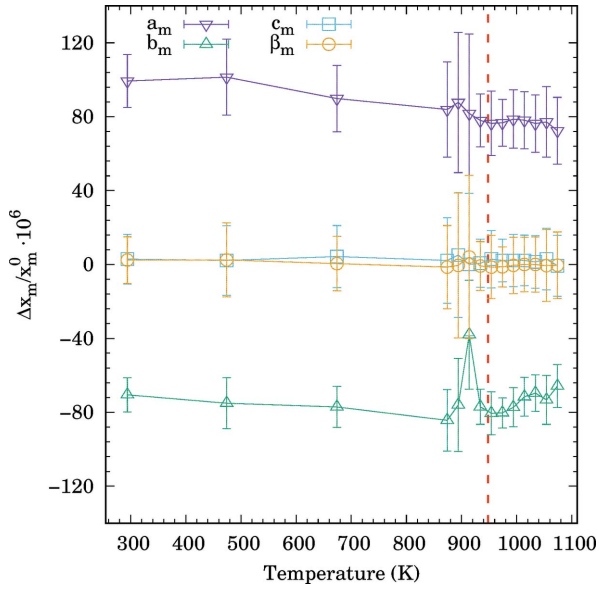

Figure 3
Temperature dependence of the relative change of the monoclinic lattice parameters a^1_m, b^1_m, c^1_m and β^1_m of α-Fe_2O_3 (see text). The vertical dotted line denotes the Néel temperature T_N = 950 K.

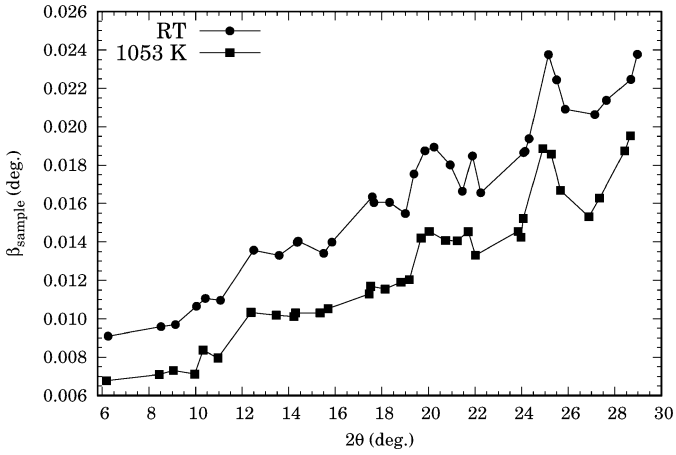

Figure 4
Angular dependence of the experimental values of the integral breadth $\beta_{sample}(2\theta)$ obtained for α-Fe_2O_3 at room temperature (Stękiel *et al.*, 2015) and 1053 K, *i.e.* above $T_N = 950$ K. The error bars were omitted for clarity and the lines are given as a guide-to-the-eye.

temperature dependence of the relative changes of the α-Fe_2O_3 monoclinic lattice parameters is shown in Fig. 3. The main conclusion of this study is that the monoclinic deformation of α-Fe_2O_3 is observed both below and above T_N.

3.2. Anisotropic peak-broadening model assuming trigonal symmetry 'on average'

The synchrotron radiation diffraction patterns of α-Fe_2O_3 measured at room temperature and 1053 K (*i.e.* above T_N) were analysed by fitting a pseudo-Voigt profile to the observed Bragg peaks (*i.e.* model-independent analysis) using *WinPlotr* (Roisnel & Rodriguez-Carvajal, 2000).

The integral breadth, denoted as $\beta_{obs}(2\theta)$ was used as a measure of the Bragg peak widths as in Williamson & Hall (1953). The instrumental contribution was estimated with the LaB_6 standard. The integral breadths obtained from the LaB_6 diffraction pattern were refined with a fourth-order polynomial function $\beta_{LaB_6}(2\theta)$. The sample contribution to the integral breadth, $\beta_{sample}(2\theta)$ was calculated as

$$\beta_{sample}(2\theta) = \{\beta^2_{obs}(2\theta) - \beta^2_{LaB_6}(2\theta)\}^{1/2}. \quad (5)$$

This formula works for Gaussian peak shape but as the instrumental contribution to β_{obs} is smooth and the use of similar fomulae, *e.g.* $\beta_{sample}(2\theta) = \beta_{obs}(2\theta) - \beta_{LaB_6}(2\theta)$, leads to the same type of *hkl*-dependent anisotropy of $\beta_{sample}(2\theta)$. The experimental $\beta_{sample}(2\theta)$ values obtained for α-Fe_2O_3 at room temperature and 1053 K are shown in Fig. 4. The lines are shown as a guide-to-the-eye. The β values observed for 1053 K are smaller than those observed at room temperature, probably because of the crystallite growth process at elevated temperatures. Similar sets of local maxima and minima of $\beta_{sample}(2\theta)$ are observed both at room temperature and 1053 K. This model independent observation confirms that the deformations of the α-Fe_2O_3 rhombohedral lattice are present both below and above T_N.

In the anisotropic peak broadening (APB) model described in Stephens (1999), the variance σ^2 of $1/d^2_{hkl}$ is calculated as:

$$\sigma^2(1/d^2_{hkl}) = \sum_{i=1}^{4} A_i W_i(h,k,l), \quad (6)$$

with the following invariant polynomials (for the assumed Laue class $\bar{3}m$): $W_1 = (h^2 + hk + k^2)^2$, $W_2 = (h^2 + hk + k^2)l^2$, $W_3 = l^4$ and $W_4 = (3h^3 - 3k^3 + (k-h)^3)l$.

The calculated integral breadths $\beta_{sample}(2\theta)$ are given as

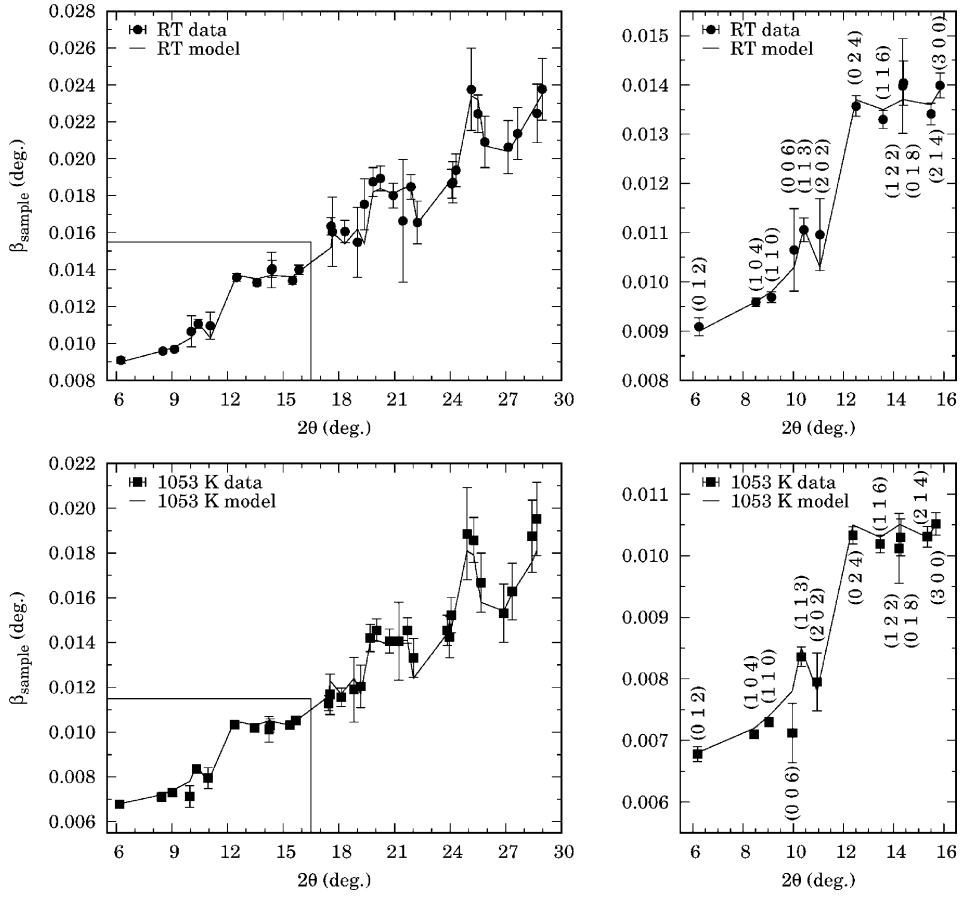

Figure 5
Angular dependence of the integral breadth $\beta_{sample}(2\theta)$ obtained for α-Fe_2O_3 at room temperature (Stękiel *et al.*, 2015) and 1053 K. The experimental values are shown with solid symbols and error bars, while results of the refinement with the APB model are shown with solid lines. The Bragg peak indices in the right panels are given for the hexagonal setting of the space group $R\bar{3}c$.

Table 5
Values of the refined parameters and their statistical accuracies obtained with the anisotropic peak-broadening model using equation (7) applied to α-Fe_2O_3 at 293 and 1053 K.

	α-Fe_2O_3 (room temperature)	α-Fe_2O_3 (1053 K)
B_0	0.0043 (2)	0.0032 (2)
A_0	4.72 (08) $\times 10^{-3}$	2.84 (39) $\times 10^{-3}$
A_2	1.36 (13) $\times 10^{-6}$	8.39 (65) $\times 10^{-7}$
A_4	-2.13 (16) $\times 10^{-6}$	-1.36 (76) $\times 10^{-6}$

$$\beta_{\rm sample}(\theta) = \frac{B_0}{\cos\theta} + \left\{A_0 + A_1\frac{W_1}{Q^4} + A_2\frac{W_2}{Q^4} + A_3\frac{W_3}{Q^4} + A_4\frac{W_4}{Q^4}\right\}^{1/2}\tan\theta. \quad (7)$$

B_0 gives the crystallite size contribution, A_0 gives the average (isotropic) microstrain-type contribution, while the coeffcients A_1, A_2, A_3, A_4 describe the anisotropic broadening contributions. The $\beta(2\theta)$ dependence observed for α-Fe_2O_3 at room temperature and 1053 K was refined using the APB model [equations (5) and (7)]. The experimental data and the calculated peak widths with the h, k, l indices (in hexagonal setting) are shown in Fig. 5. The resulting coefficients A_i [see equation (7)] are given in Table 5. The coefficients A_1 and A_3 give values smaller than their statistical errors. Setting $A_1 = A_3 = 0$ did not change the fit quality in a significant way. It is interesting to note that the coefficient $A_4 < 0$. With positive l, the polynomial $W_4 = (3h^3 - 3k^3 + (k-h)^3)l$ gives positive values for $h > k$ and negative for $h < k$. The contribution of W_4 with the negative coefficient A_4 explain the 'reversed' behaviour of the widths of the broad (0, 2, 4) and the narrow (2, 0, 2) Bragg peaks, see Fig. 5. The polynomial W_4 gives zero for (h, h, l) so the behaviour of the widths of *e.g.* (1, 1, 3), (1, 1, 6) Bragg peaks is described with the positive coefficient of the polynomial $W_2 = (h^2 + hk + k^2)l^2$.

4. Discussion

The present paper shows that the high-resolution synchrotron radiation diffraction patterns of α-Fe_2O_3 can be described by assuming either (i) a monoclinic symmetry of the crystal structure or alternatively (ii) a statistically described deformation of the rhombohedral lattice (so-called APB model; Stephens, 1999). The deformation resulting from the APB obtained with the negative A_4 coefficients (see Table 4) indicates a breaking of the trigonal symmetry. This is because $A_4 \neq 0$ implies a non-orthogonality between the pseudo-hexagonal axes $\mathbf{c}_{\rm h}^1$ with $\mathbf{a}_{\rm h}^1$ as well as $\mathbf{c}_{\rm h}^1$ with $\mathbf{b}_{\rm h}^1$. In this case the threefold rotation axis is absent in the symmetry of the crystal structure of α-Fe_2O_3.

The proposed monoclinic crystal structure (space group $C2/c$) leads to Bragg peaks that are forbidden in the rhombohedral structure (space group $R\bar{3}c$). The intensities of 25 such forbidden Bragg peaks calculated using the structural parameters from Tables 2–4 are shown in Table 6. The Bragg peaks allowed in the monoclinic model but forbidden in the rhombohedral model are numbered from 1 to 25. A few representative Bragg peaks allowed in the rhombohedral model are also shown. The most intense rhombohedral Bragg peak $(104)_{\rm h}$ has a total intensity of 2×10^6, while the most intense forbidden peaks have intensities of about 500. A measurement of weak reflections (*i.e.* 4000 times weaker than the most intense reflection) was not possible at the high-resolution synchrotron radiation diffraction beamline ID22, *i.e.* they are too weak compared with the background fluctuations in the experimental data. The present data gives no hint on the possible temperature dependence of these forbidden reflections. The forbidden reflections due to the monoclinic deformations discussed above should not be confused with the forbidden hexagonal $(003)_{\rm h}$ and $(009)_{\rm h}$ reflections studied by resonant synchrotron scattering in hematite, see *e.g.* Finkelstein *et al.* (1992) and Carra & Thole (1994). The monoclinic Bragg peaks $(\bar{2}03)_{\rm m}$ [equivalent to $(003)_{\rm h}$] and $(\bar{6}09)_{\rm m}$ [equivalent to $(009)_{\rm h}$] are also both forbidden in the space group $C2/c$.

Table 6
List of Bragg peak intensities calculated for the monoclinic α-Fe_2O_3 crystal structure model for 293 and 1053 K (parameters from Table 4).

The first column gives the peak number (for peaks forbidden in the rhombohedral model) or the hexagonal indices (for peaks allowed in the rhombohedral model). Columns 2–4 give the monoclinic indices, columns 5–6 and 7–8 give the d-spacings and intensities calculated for 293 and 1053 K, respectively.

1 No.	2 h	3 k	4 l	5 d(293 K) (Å)	6 I(293 K)	7 d(1053 K) (Å)	8 I(1053 K)
1	−1	1	1	4.157220	538.4	4.198735	478.5
$(012)_{\rm h}$	−2	0	2	3.683574	212434.0	3.717948	198030.1
$(012)_{\rm h}$	−1	1	2	3.682504	368969.3	3.717051	350127.5
$(104)_{\rm h}$	−3	1	4	2.700070	1355721.9	2.722419	1352078.9
$(104)_{\rm h}$	−2	0	4	2.699572	664717.6	2.722078	640748.8
$(110)_{\rm h}$	1	1	0	2.518051	995831.4	2.543982	947777.1
$(110)_{\rm h}$	0	2	0	2.517771	482353.1	2.543684	476386.6
2	−3	1	5	2.326172	10.7	2.344772	127.6
$(006)_{\rm h}$	−4	0	6	2.291931	33734.0	2.308114	27871.0
3	0	2	1	2.153576	241.8	2.175587	473.4
4	−5	1	7	1.791271	79.7	1.804867	10.6
5	−4	2	5	1.708799	193.2	1.724219	127.5
6	−4	2	7	1.459420	15.8	1.471864	112.4
7	−3	3	3	1.385740	15.1	1.399578	5.1
8	−1	3	3	1.385616	13.6	1.399484	4.7
9	−7	1	11	1.201693	0.5	1.210484	10.1
10	−2	4	1	1.086870	26.6	1.098033	11.3
11	−8	2	11	1.084616	42.9	1.093121	9.3
12	−7	3	9	1.053271	4.8	1.062471	1.4
13	−5	3	9	1.053107	3.5	1.062348	1.0
14	−9	1	13	1.028041	12.8	1.035474	0.2
15	−2	4	5	1.013482	14.4	1.023481	9.3
16	−6	4	7	0.953360	18.9	0.962430	4.7
17	−8	2	13	0.951677	0.2	0.958996	16.2
18	1	5	1	0.870456	37.2	0.879408	49.6
19	−5	5	5	0.831444	42.4	0.839747	34.8
20	−3	5	7	0.797129	18.2	0.804920	35.6
21	−11	1	17	0.795328	0.8	0.801035	1.7
22	−11	3	15	0.775499	1.5	0.781672	0.3
23	−9	3	15	0.775390	0.9	0.781590	0.2
24	−10	4	13	0.759260	9.5	0.765794	1.2
25	−12	2	17	0.758450	14.7	0.764091	0.9

The most important conclusion from this study is that the crystal structure of α-Fe_2O_3 is monoclinic both below and above T_N. The monoclinic symmetry may be related with the magnetic properties of α-Fe_2O_3. These observations should be compared with the oxidation of iron which leads to the formation of α-Fe_2O_3 nanowires (Fu *et al.*, 2001; Wen *et al.*, 2005; Yuan *et al.*, 2012). These nanowires grow along the unique monoclinic $\mathbf{b}_m$ axis, *i.e.* hexagonal [110] direction and the whole process occurs at temperatures from 873 to 1073 K, *i.e.* both below and above the bulk α-Fe_2O_3: T_N = 950 K. Although the crystal structure of α-Fe_2O_3 nanowires is reported to be trigonal (Fu *et al.*, 2001; Wen *et al.*, 2005; Yuan *et al.*, 2012), the growth direction anisotropy points towards the monoclinic symmetry hypothesis for nanowires as well. On the other hand, the monoclinic symmetry can also be unrelated with the magnetic properties; a recent study has shown similar monoclinic crystal structure symmetry in the nonmagnetic calcite, $CaCO_3$ (Przeniosło *et al.*, 2016). These findings show the need for further studies of α-Fe_2O_3 in the vicinity of its Néel transition.

Acknowledgements

Thanks are due to A. Fitch for support during the measurements at ESRF. Thanks are due to the Ministry of Science and Higher Education (Poland) for funding access to the ESRF facilities.

References

Brown, P., Forsyth, J., Lelièvre-Berna, E. & Tasset, F. (2002). *J. Phys. Condens. Matter*, **14**, 1957–1966.
Brown, P., Forsyth, J. & Tasset, F. (1999). *Physica B*, **267–268**, 215–220.
Caglioti, G., Paoletti, A. & Ricci, F. (1958). *Nucl. Instrum.* **3**, 223–228.
Carra, P. & Thole, B. (1994). *Rev. Mod. Phys.* **66**, 1509–1515.
Dzyaloshinsky, I. (1958). *J. Phys. Chem. Solids*, **4**, 241–255.
Finkelstein, K., Shen, Q. & Shastri, S. (1992). *Phys. Rev. Lett.* **69**, 1612–1615.
Fu, Y., Chen, J. & Zhang, H. (2001). *Chem. Phys. Lett.* **350**, 491–494.
Grimmer, H. (2015). *Acta Cryst.* A**71**, 143–149.
Hill, A. H., Jiao, F., Bruce, P. G., Harrison, A., Kockelmann, W. & Ritter, C. (2008). *Chem. Mater.* **20**, 4891–4899.
Landau, L. & Lifschitz, E. (1969). *Statistical Physics.* Oxford: Pergamon Press.
Maslen, E. N., Streltsov, V. A., Streltsova, N. R. & Ishizawa, N. (1994). *Acta Cryst.* B**50**, 435–441.
Morin, F. J. (1950). *Phys. Rev.* **78**, 819–820.
Moriya, T. (1960). *Phys. Rev. Lett.* **4**, 228–230.
Morrish, A. H. (1994). *Canted Antiferromagnetism: Hematite.* Singapore: World Scientific.
Néel, L. & Pauthenet, R. (1952). *C. R. Acad. Sci.* **234**, 2172–2174.
Petrás, L., Preisinger, A. & Mereiter, K. (1996). *Mater. Sci. Forum*, **228–231**, 393–398.
Petříček, V., Dušek, M. & Palatinus, L. (2014). *Z. Kristallogr.* **229**, 345–352.
Przeniosło, R., Fabrykiewicz, P. & Sosnowska, I. (2016). *Physica B*, **496**, 49–56.
Przeniosło, R., Sosnowska, I., Stękiel, M., Wardecki, D., Fitch, A. & Jasiński, B. (2014). *Physica B*, **449**, 72–76.
Roisnel, T. & Rodriguez-Carvajal, J. (2000). *Mater. Sci. Forum*, Proc. 7th European Powder Diffraction Conference, EPDIC, 7, 118–123.
Shull, C. G., Strauser, W. A. & Wollan, E. (1951). *Phys. Rev.* **83**, 333–345.
Sosnowska, I., Neumaier, T. P. & Steichele, E. (1982). *J. Phys. C*, **15**, 4835–4846.
Sosnowska, I., Przeniosło, R., Palewicz, A., Wardecki, D. & Fitch, A. (2012). *J. Phys. Soc. Jpn*, **81**, 0446041–4.
Stękiel, M., Przeniosło, R., Sosnowska, I., Fitch, A., Jasiński, J. B., Lussier, J. A. & Bieringer, M. (2015). *Acta Cryst.* B**71**, 203–208.
Stephens, P. W. (1999). *J. Appl. Cryst.* **32**, 281–289.
Wen, X., Wang, S., Ding, Y., Wang, Z. & Yang, S. (2005). *J. Phys. Chem. B*, **109**, 215–220.
Williamson, G. & Hall, W. (1953). *Acta Metall.* **1**, 22–31.
Yuan, L., Wang, Y., Cai, R., Jiang, Q., Wang, J., Li, B., Sharma, A. & Zhou, G. (2012). *Mater. Sci. Eng. B*, **177**, 327–336.